Statistical Models for Retrieval of Himalayan Land Surface Parameters for Geomorphologic Research

Manjeet Singh[1], V. D Mishra[2], N. K Thakur[3], Jyoti Dhar Sharma[4]

[1, 4]Department of Physics, Shoolini University
Solan (H.P) -173212, India
thakur.m82@gmail.com

[2,3]Snow & Avalanche Study Establishment, Defense research and Development Organization,
Chandigarh (U.T)-160036, India
vd_mishra@rediffmail.com

Abstract: ***Qualitative and quantitative estimation of land surface parameters has great concern for ecological and hydrological system. This makes land surface parameters as an important tool to study earth's climate system especially when satellite data provide timely and efficient information about large land area. In the present paper, the study was carried out by using NASA's hyper spectral EO-1 Hyperion sensor and multi-spectral Advance Wide Field Sensor (AWiFS) of IRS-P6 for different ranges (lower, middle and upper) of Himalaya. The analysis procedure consists of Fast Line-of-sight Atmospheric Analysis of Spectral Hyper cubes (FLAASH) atmospheric correction code derives its physics-based algorithm from the Moderate Resolution Transmittance (MODTRAN4) radiative transfer code as well as radiometric (atmospheric + topographic) correction to retrieve surface reflectance. The terrain characteristics have been extracted from Digital Elevation Model (DEM) using 1:50,000 scale SoI maps at 40m contour interval. Various statistical models for supervised classification such as spectral angle mapper (SAM), support vector machine (SVM), and maximum likelihood (MLH) has been examined and validated with existed Normalized Difference; Vegetation Index (NDVI), Snow Index (NDSI) and Glacier Index (NDGI) models. The spectral reflectance of different surface parameters has been collected in field, using spectro-radiometer and compared with satellite derived spectra. Present work has focused on three key issues (a) accurate registration of the images for land cover maps (b) estimation of spatial distribution of snow cover at sub pixel level and (c) multi-temporal input to hydrological, ecological and land surface modeling. Study distills these statistical approaches into a unique set of hierarchical taxonomy that reveals the similarities and differences between algorithms.***

Keywords: AWiFS, Hyperion, FLAASH, SAM, MLH and SVM

1. Introduction

Hydrological cycle and ecological system are generally affected by the level and type of land surface parameters such as land covers which includes: snow, water, grassland, forest, and bare soil [1]. And extraction of surface parameters has world-wide concern to understand its impact on radiation balance, local climate, global climate change, biogeochemistry, diversity and abundance of terrestrial species. Thus an accurate representation of surface parameters and biophysical attributes (soils, elevation, topography-slope and aspect, etc.) of the landscape within Himalaya is required [2]. In the last three decades, considerable advancement in space technology providing a numerous satellite platforms to study complex physical processes of the earth-atmosphere system [3]. And one of the best basic characteristics of remote sensing is the extensive use of quantitative algorithms for estimating earth surface variables [4]. The accurate estimation of surface variable using coarse resolution satellite sensor is challenging task due to mixing of various heterogeneous land features in a pixel. Sub-pixel classification techniques using multispectral data have been reported by many authors [5], [6] to improve the accuracy of classification for many applications in the field of earth surveys. However, for certain applications there is a limit in the spatial and spectral resolution of satellite sensor which restricts the usefulness of multispectral data [7].

To get full advantages of spatial and spectral resolution, hyper spectral imagery EO-1 Hyperion and medium resolution AWiFS sensor provides opportunities to extract more detailed information than traditional multispectral data. The main objective of the present paper is to extract land surface parameters for different ranges of Himalayas with varying altitude from 1100m to 6000m. Various statistical models for supervised classification such as spectral angle mapper (SAM), support vector machine (SVM), and maximum likelihood (MLH) has been examined and compared/validate with existed models.

2. Study area

The study area is divided in three different zones of Himalaya. 1st study area is located in Pir-Panjal range of lower Himalayan Zone [8] lies at $32^0$11'25''N-$32^0$26'28''N latitude and $77^0$0'21''E-$77^0$20'25''E longitude. The area is thickly forested covered maximum with coniferous trees in the lower altitude along the valley and its average altitude varies from 1100m to 5000 m [9]. This lower Himalayan zone is adjacent to the 2nd study area, that lies at $32^0$11'40''N-$32^0$17'46'' N latitude and $78^0$30'13''E-$78^0$30'14''E longitude in middle (greater) Himalayan Zone which is characterized by fairly cold temperatures, heavy snowfall and higher elevations. And the 3rd study area is located in the Karakoram Range of upper Himalayan Zone lies between $35^0$42'7''N-$35^0$48'13''N and $76^0$20'5''E-$76^0$20'6''E. The majority of the slopes inclination lies in the range of 55-60 degree. Figure 1 shows different study area on SoI map and on different satellite images.

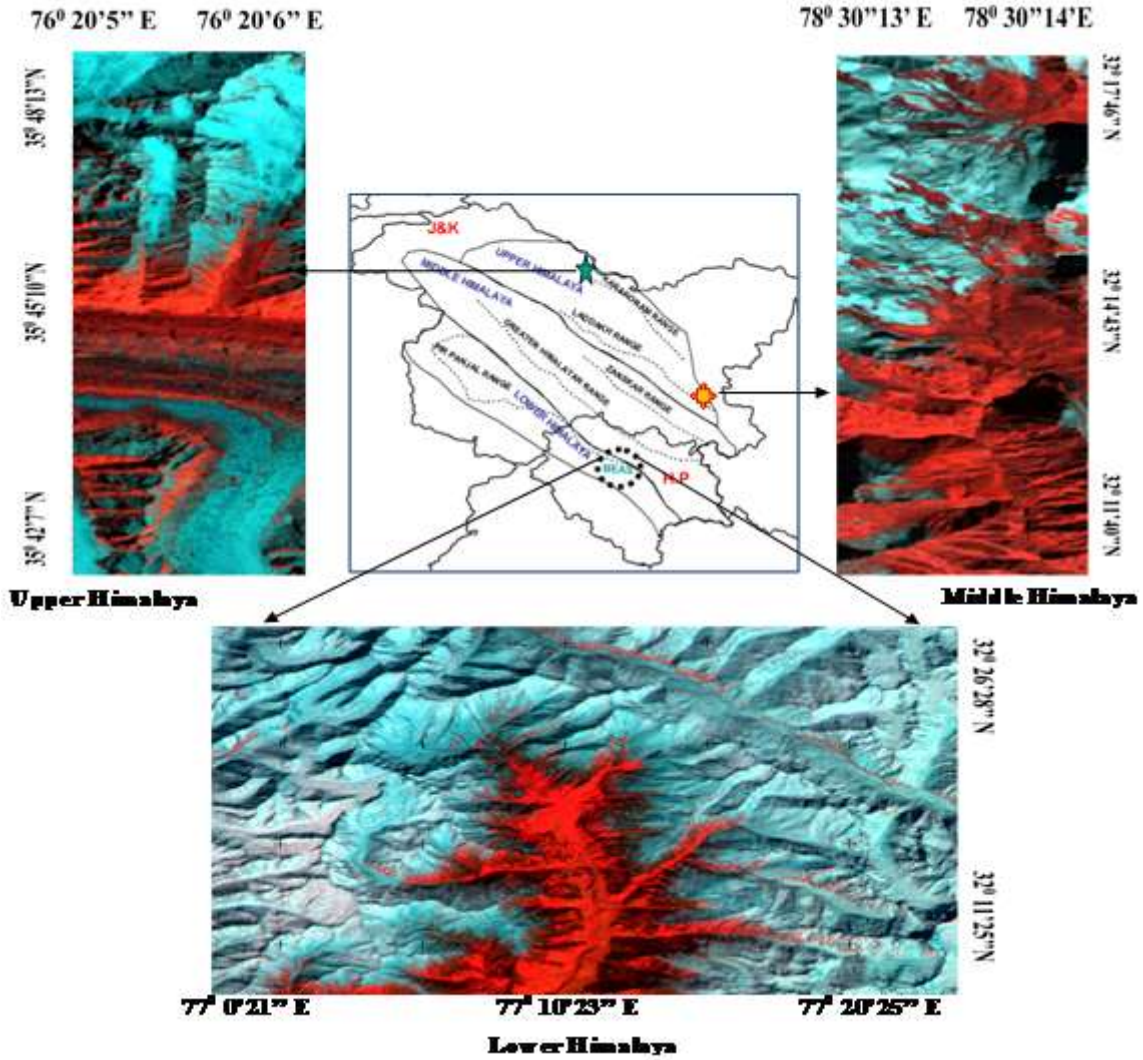

Figure 1: Study area on India Map with different ranges of Himalaya and AWiFS-Hyperion satellite images of Lower, Middle and Upper Himalaya

Table 1: Salient specification of IRS-P6_AWiFS Sensor

Band No	*Spectral Bands (nm)*	*Spatial Resolution at Nadir (m)*	*Quantization (bit)*	*Radiance ($mWcm^{-2}Sr^{-1}\mu m^{-1}$)*		*Mean solar Exo-atmospheric spectral irradiance ($mWcm^{-2}\mu m^{-1}$)*
				Minimum	Maximum	
B1	520-590	56	10	0	52.34	185.3218
B2	620-680	56	10	0	40.75	158.042
B3	770-860	56	10	0	28.425	108.357
B4	1550-1700	56	10	0	4.645	23.786

2.1 AWiFS

Study on lower Himalayan Zone was carried out with multi-temporal Advance Wide Field Sensor (AWiFS) of RESOURCESAT-1 dated 24-December-2008 and 11-March-2009. AWiFS scans a 740 km wide swath, acquiring data in 4 bands including Visible (Green and Red), NIR and SWIR. Its spatial resolution is 56m at Nadir. Its radiometric resolution is 10 bit, which does not saturate over snow. The salient specifications of AWiFS sensor is given in Table 1.

2.2 EO-1 Hyperion

The study at middle and upper Himalayan Zone was carried out with Level 1_A: L1G/L1T data (geometric and terrain corrected) of Hyperion sensor onboard NASA's Earth Observing one (EO -1) platform. Hyperion collects 220 unique spectral channels ranging from 357nm to 2576nm with a 10-nm bandwidth [10]. The instrument operates in a push broom fashion, with a spatial resolution of 30 meters for all bands with a standard scene width of 7.7 kilometers. The data is available in 16-bit signed integer's radiance values.

3. Methodology

3.1 Satellite data processing

All the AWiFS images were geo-referenced to the Everest datum in ERDAS/ Imagine 9.1 (Leica Geosystems GIS & Mapping LLC) with sub-pixel accuracy using nearest neighborhood re-sampling technique. A DEM of the study area was generated using 1:50,000 survey of India (SoI) toposheet at 40m contour level. Whereas Hyperion images are geometric and terrain corrected [10] covered the wavelength region by two detector arrays, one for the visible and near -infrared (VNIR: 356 nm to 1058 nm) and other for short-wave infrared (SWIR: 852 nm to 2577 nm) with 242 bands of 10 nm spectral resolution and 30 m spatial resolution [10]**.** But due to radiometric detraction and signal to noise issues only 198 bands are calibrated [11]. The detail description of radiometric errors in Hyperion data are reported by Bindschadler (2003) [12]**.** As a result, only a subset of 158 bands maintained for further analysis. Hyperion satellite data was pre-processed in ENVI 4.7 software [13]**.** The flow chart of the detailed methodology is given in figure 2.

3.2 Radio metrically corrected reflectance

3.2.1 For AWiFS image

Image-based atmospherically corrected target spectral reflectance on the tilted surface, $R_{\lambda T}$, from sensor radiance, L_λ, is obtained using the following model [14], [15]:

$$R_{\lambda T} = \frac{\pi(L_\lambda - L_p)d^2}{t_v(E_0 \cos\theta_z t_z + E_d + E_t)}$$

Where L_p is the path radiance in $mWcm^{-2}sr^{-1}\mu m^{-1}$ [16] and d is the Earth–Sun distance in astronomical units [17]. E_0 is band pass exoatmospheric spectral irradiance (Table. 1), E_d is down welling spectral irradiance at the surface due to diffused radiation and assumed equal to zero [18], θ_z is the solar zenith angle [19] and calculated for each pixel of the study area, t_v is atmospheric transmittance along the path from ground surface to sensor and t_z is atmospheric transmittance along the path from Sun to ground calculated for the AWiFS spectral bands using the model [14]. The parameter E_t is the terrain irradiance contributed due to reflected radiation from the adjacent terrain. It is not considered in the present work for AWiFS data because the effect needs to be included only with fine spatial resolution [20]. Nichol (2006) [21] proposed topographic correction in two stages in order to enhance the results on north facing slopes in the shadow area, equalization of radiance is required with respect to Sun- facing slopes to make the extent of corrections equal to the maximum difference of radiance values on both aspects. Advantages of this method, especially for Himalayan rugged terrain using AWiFS has been reported by Mishra (2010) [7].
The final corrected reflectance is estimated by the following equation [21]:

$$R_{n\lambda ij} = R_{\lambda ij} + (R_{max} - R_{min})\frac{[(\langle \cos i \rangle s - \cos_{ij} i)]c_\lambda}{\langle \cos i \rangle s}$$

Where $R_{n\lambda ij}$ is the normalized reflectance values for image pixel ij in waveband λ, $R_{\lambda ij}=R_{\lambda T}$ is the uncorrected original reflectance on the tilte s, cos i his is the scaled (0–255) mean IL on the south aspect and C_λ is the coefficient estimated for each AWiFS and MODIS spectral band using the equation proposed by Nichol (2006) [21].

3.2.2 For EO-1 Hyperion

Atmospheric effects caused by molecular, particulate scattering and absorption from the 'radiance-at-detector has been eliminated by using Fast Line-of-sight Atmospheric Analysis of Spectral Hyper cubes (FLAASH) module based on the MODTRAN-4 radiative transfer code [22], [23] in order to retrieve 'reflectance-at-surface' values. FLAASH allows a researcher to define all parameters that influence atmospheric absorption and scattering such as relative solar position, aerosol, and scattering models, visibility parameters, ozone total vertical column, adjacency effects (scattering of reflected radiance from surroundings into a pixel), artifact suppression [24] and provides water vapor retrieval. In the present study, atmospheric model with 2-band KT aerosol model [25] was used for atmospheric correction.

Digital values in Hyperion data represent absolute radiance ($W/m^2*\mu m*sr$) values stored as 16-bit signed integers with a scaling factor of 40 for VNIR bands and 80 for SWIR bands. The spectral radiance at sensor pixel using FLAASH is derived from a standard equation [23] as:

$$L = Lgi + Lpi$$

$$Lgi = A\frac{\rho}{1-\rho iS} \text{ and } Lpi = B\frac{\rho i}{1-\rho iS} + La$$

Where Lgi is the at-sensor radiance reflected by the target and Lpi is the at-sensor radiance scattered into the path by the atmosphere and the surrounding targets, (ρ) is the pixel surface reflectance, (ρ_i) is an average surface reflectance for the pixel and a surrounding region, (S) is the spherical albedo of the atmosphere and (La) is the radiance back scattered by the atmosphere. The coefficient A and B depends on atmospheric and geometric conditions but not on the surface. Each of these variables depends on spectral channels; the wavelength index has been omitted for simplicity.

The values of A, B, S and La are determined from MODTRAN4 calculations that use the viewing and solar angles and the mean surface elevation of the measurement, and they assume a certain model atmosphere, aerosol type, and visible range.

3.3 Surface parameters extraction

3.3.1 Normalized difference Vegetation Index (NDVI)

Efficiency of NDVI in land cover classification, forest covers mapping and vegetation analysis has been reported by Justice (1985) [26].

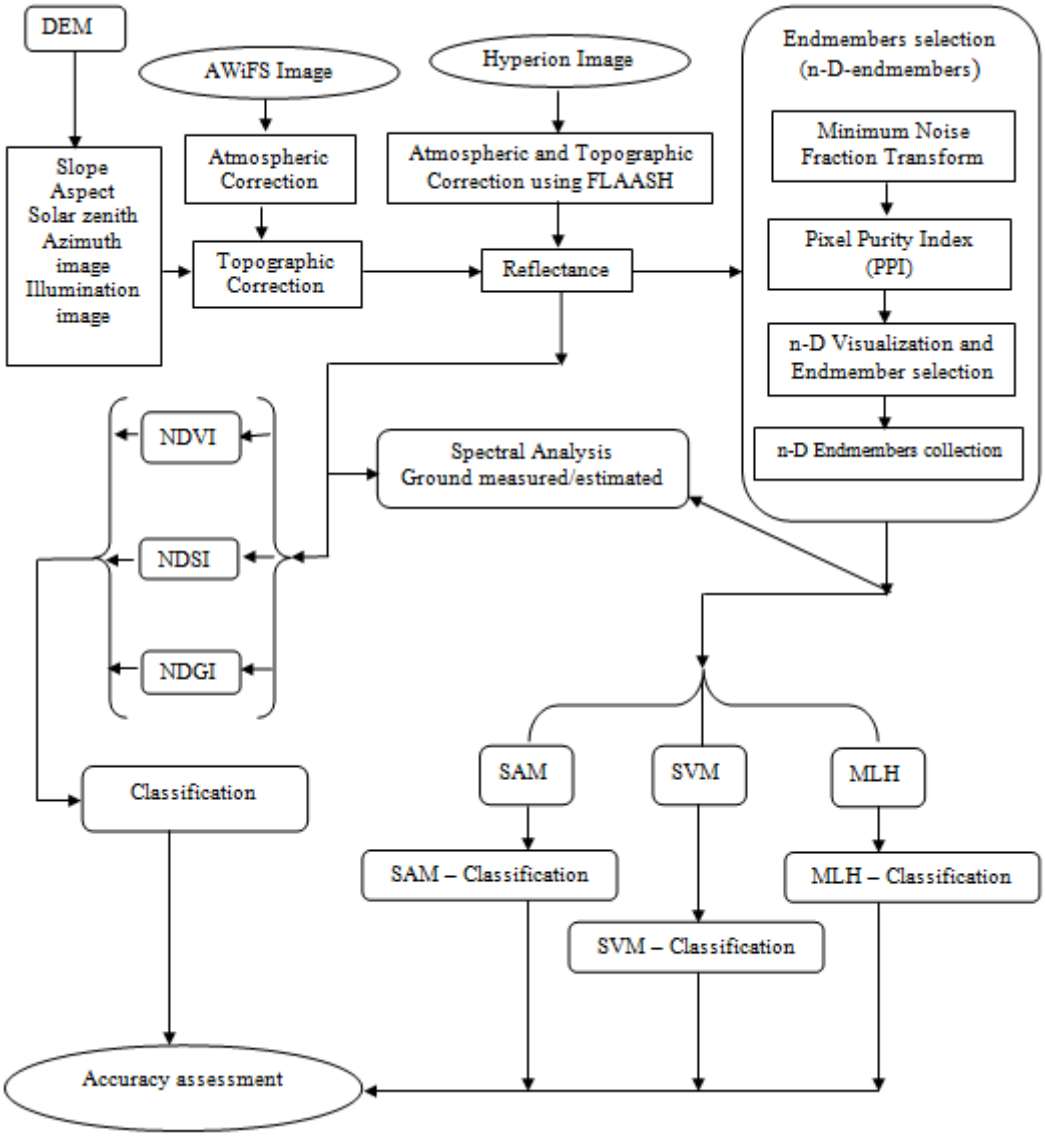

Figure 2: Flow chart summarizing the methodology followed in the study

$$NDVI = \frac{(R_{NIR} - R_{Red})}{(R_{NIR} + R_{Red})}$$

$-1 \leq NDVI \leq 1$ value distribution has used in the study to standardize vegetation and non-vegetation area.

3.3.2 Normalized Difference Snow Index (NDSI)

Hall (1995) proposed Normalized Difference Snow Index (NDSI) method to identifying snow cover area and defined [27] as:

$$NDSI = \frac{(R_{Green} - R_{SWIR})}{(R_{Green} + R_{SWIR})}$$

Here, "R_{Green}" is the reflectance of the visible band (0.52 – 0.60 µm) and "R_{SWIR}" is the reflectance of the short wave infrared band (1.55-1.75 µm). The specific threshold value of NDSI of 0.4 is defined to allow identification of snow covered areas from images produced by different sensors [28]. The water body also has high positive NDSI values and merges with snow cover area. Hence the water body was masked using the reflectance of NIR band >10 % and the NDSI >= 0.4 [9]. A.K Keshri (2009) reported the advantages of NDSI to discriminate 'Snow+ice+ice mixed debris' surfaces from debris [29].

3.3.3 Normalized Difference Glacier Index (NDGI)

Further discrimination within 'Snow+ice+IMD' surfaces has been recognized by standard equation of Normalized Difference Glacier Index (NDGI) [29] and defined as:

$$NDGI = \frac{(R_{Green} - R_{Red})}{(R_{Green} + R_{Red})}$$

The specific threshold value 0.025 has been chosen for the study area data set.

3.4 Land Cover Classification

3.4.1 Spectral angle mapper (SAM)

A physically-based classification spectral angle mapper (SAM) method was used in present study for the land-

surface parameter extraction. The algorithm determines the spectral similarity between the two spectra (i.e. the pixel spectra to known/reference spectra) by calculating the angle between two vectors representing these spectra [30].

3.4.2 Maximum likelihood (MLH)

Maximum likelihood classification assumes that the statistics for each class in each band are normally distributed and calculates the probability that a given pixel belongs to a specific class. Each pixel is assigned to the class that has the highest probability (that is, the maximum likelihood). ENVI implements maximum likelihood classification by calculating the discriminant functions for each pixel in the image [31].

3.4.3 Support Vector Machine (SVM)

To perform supervised classification on images, support vector machine (SVM) is used to identify the class associated with each pixel. It separates the classes with a decision surface that maximizes the margin between the classes. Present classification was done with SVM radial basis function (RBF) kernel. This kernel nonlinearly maps samples into a higher dimensional space so it can handle the case when the relation between class labels and attributes is nonlinear. Mathematical representation of radial basis function (RBF) kernel [32] is listed as

$$K(x_i, x_j) = \exp(-\gamma \|x_i - x_j\|^2), \gamma > 0$$

Where γ is the gamma term in the kernel function for all kernel types except linear. To evaluate all above selected methodology and classification results, the selection of end members based on "Spectral Hourglass" processing scheme [30] were implemented. This Procedure includes the generation of Minimum Noise Fraction-Images (MNF) for data dimensionality estimation and reduction by de correlating the useful information and separating noise [33], Pixel Purity Index-Mapping (PPI) for the determination of the purest pixels in an image (as potential end members) utilizing the (uncorrelated) MNF-images and finally the extraction of end members utilizing the n-Dimensional-Visualizer tool (Figure 3). The extracted end member's spectra are then compared with the in-situ measured spectral reflectance using optical spectro-radiometer (Figure 4a, 4b).

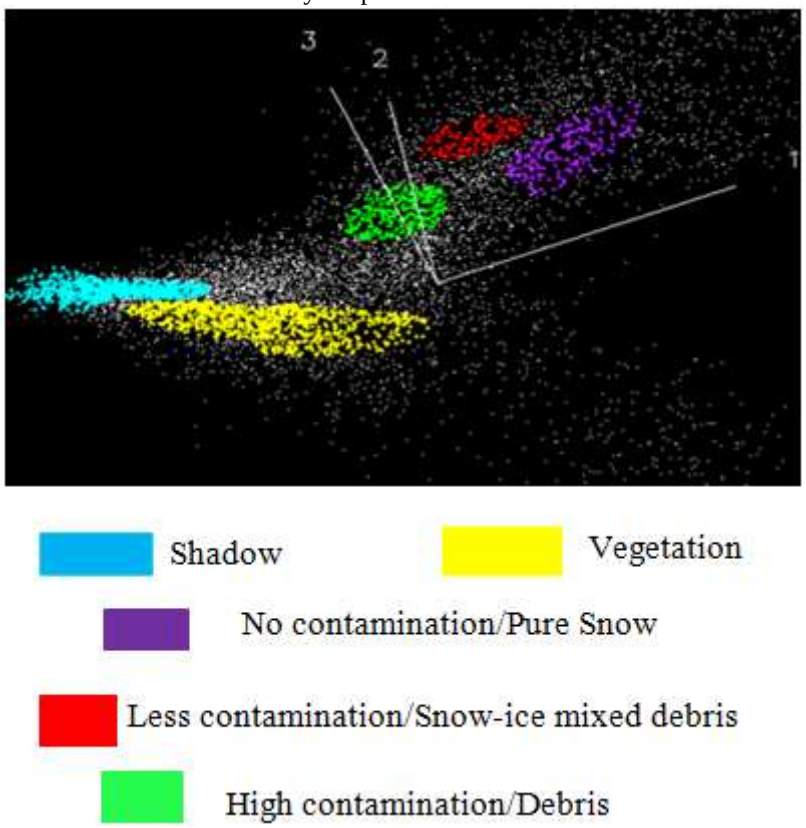

Figure 3: 3-D visualization for end member's selection of different classes in Hyperion data (3-May-2011)

The selected image spectra end members were further used as reference spectra for various surface parameters using SAM, MLH and SVM method. The threshold value of SAM angle for classification was set after iteration for tuning the angle between the pixel spectra and the reference spectra to avoid misclassification especially in the shadow regions.

4. Results

4.1 Spectral analysis

In-situ observations of spectral reflectance using optical spectro-radiometer on the same day at the time of satellite pass over the study area are collected at number of points for pure snow, soil, vegetation, water, less contaminated snow (vegetation/soil mixed snow) samples (Figure 4a, 4b) and AWiFS spectral reflectance (11 Mar 2009) using Lambertian

assumption model (Figure 4c) are now compared with in-situ observations. Due to non-availability of any image data with spatial resolution higher than 15m and inaccessible region at middle and upper Himalaya, Hyperion visible/near-infrared image was itself used as reference data. The test sample constituting 50 pixels per class was collected and reference class values to each point were given on the basis of analysis of spectral curves (Figure 4d) which were compared with in-situ measured spectral reflectance at lower Himalaya.

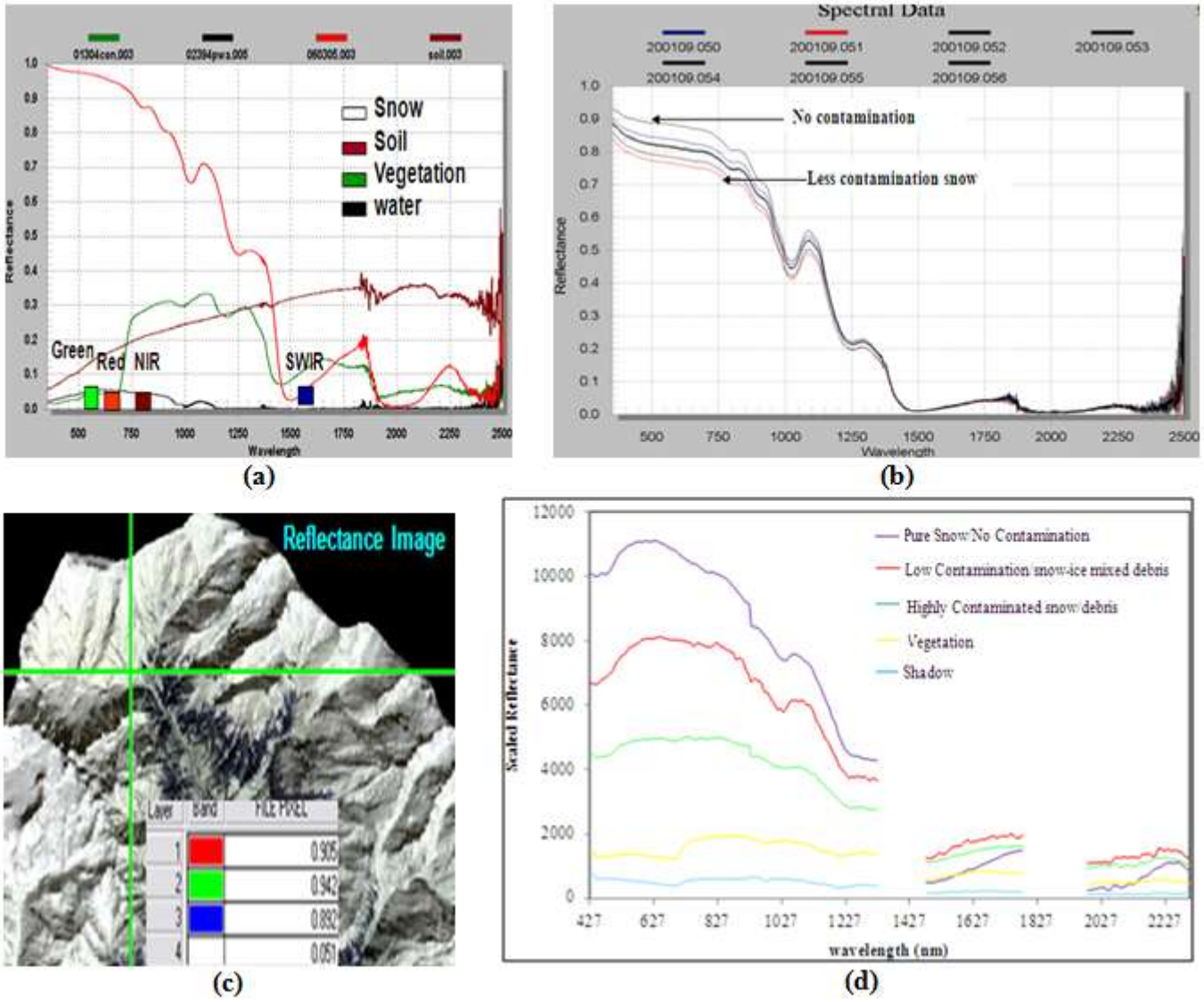

Figure 4: (a-b) In situ measured spectral reflectance (11 Mar 2009) at Lat/log: $32^0$21''33''N/$77^0$7''43''E (c) AWiFS derived spectral reflectance (d) Hyperion derived spectral reflectance

4.2 Retrieval of Land surface parameters

A sequential classification of Himalayan land surface parameters such as pure snow/no contamination, less contaminated snow/snow-ice mixed debris, debris, soil and vegetation has retrieved with various statistical models (Figure 5). The comparative visual analysis of AWiFS and Hyperion for different dates obtained using SAM, SVM and MLH is shown in figure 5 ((g-l), (m-r) and (s-x)). In order to confirm the actual land cover area after atmospheric and topographic correction, the results are compared with existed methods (Figure 5 (a-f)) estimated for both sensors.

Mostly the shady areas in all ranges of Himalayas are unclassified with SAM technique. On the other hand MLH technique over classifying the surface parameters, whereas the appearance of different land covers using SVM (Figure 5 (m-r)) are quite similar with existed models (Figure 5 (a-f)).

Figure 5 shows the thematic results of various land surface parameters.

4.3 Statistical analysis and Validation

For the purpose of validation the classified output, a statistical matrix-based approach is developed between existed and proposed models (Table 2). Regression analysis for different dates (Figure 6) of Hyperion data as well as tabular matrix approach (Table 2(a-d)) supporting the strength of SVM as an additional tool to retrieve land surface parameters at lower, middle and upper Himalaya. Classification is not complete unless error analysis has been performed.

In this paper, the root mean square error (RMSE) is calculated as follows [34]

$$\text{RMSE} = \sum_{i=1}^{M} \sqrt{\frac{1}{M}\sum_{j=1}^{n}\left(\frac{e_c^2}{n^2}\right)}$$

Where M is the no. of bands and n is the no. of pixels. RMSE values of SVM Model are found to be low as comparative to SAM and MLH as shown in Table 3.

5. Conclusion and Discussion

The present paper discusses qualitative and quantitative analysis of various statistical methods on AWiFS and Hyperion satellite data. Band ratios and vegetation index provides useful information in characterizing land covers and enhance land-cover mapping**.** Himalayan land-surface parameters such as pure snow/no contamination, less contaminated snow/snow-ice mixed debris, debris, soil and vegetation has retrieved from various statistical models (SAM,SVM and MLH) and compared with existed models for different ranges (lower, middle and upper) of Himalayas. The SAM and MLH methods are not very successful in Himalayan regions and produce poor results. Mostly the shady areas in all ranges of Himalayas are unclassified with SAM technique. Extracted land surface parameters using SVM are quite similar in texture and areas on comparing with existed models. In few places, using SVM there is a small deviation which may be due to the selection of threshold values used for the conversion of indices to surface classes. It is important to note that the threshold values are likely to be scene dependent and empirical analysis may be necessary for each case. Hence the study reveals the suitability of SVM model for the different ranges of Himalayas for (i) accurate extraction of land surface parameters (ii) snow cover distribution at sub-pixel level (iii) can provide multi-temporal inputs to various hydrological, ecological and land surface modeling.

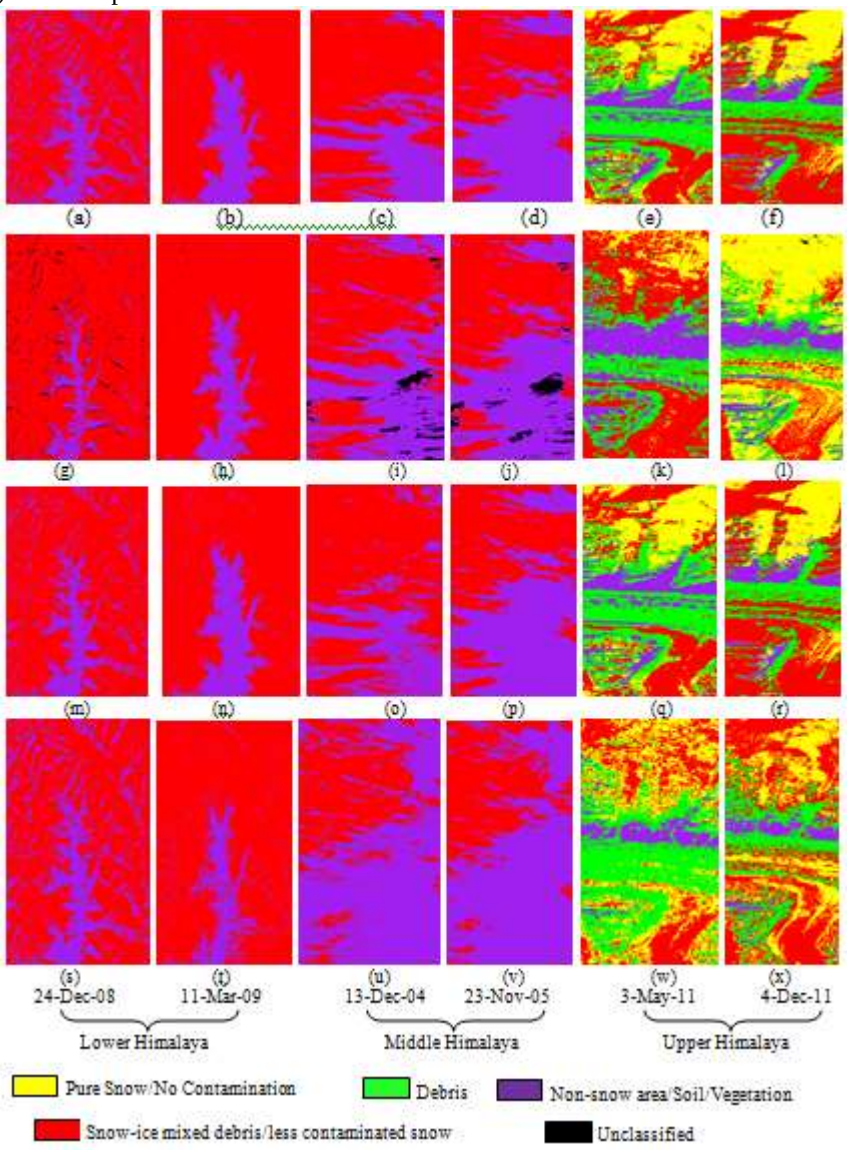

Figure 5: Thematic maps of land surface parameters using (a-f) existed models, (g-l) SAM, (m-r) SVM and (s-x) MLH

Table 2 (a): Land covers classification in (% age) with various statistical models

Study Area	*Date/Month/ Year*	*Land Cover Classification in % age (with existed models)*			
		No contamination/ Pure Snow	*Less Contaminated Snow/Snow-ice mixed debris*	*Debris*	*Non-Snow area/Soil/ Vegetation*
Lower Himalaya	24-Dec-2008	0	78.44	0	21.56
	11-Mar-2009	0	81.73	0	18.27
Middle Himalaya	13-Dec-2004	0	68.63	0	31.37
	23-Nov-2005	0	45.75	0	54.25
Upper Himalaya	03-May-2011	22.98	28.12	34.12	14.78
	04-Dec-2011	21.02	46.60	22.26	10.12

Table 2 (b): Land covers classification in (% age) with various statistical models

Study Area	*Date/Month/Year*	*Land Cover Classification in % age (with SAM)*				
		No contamination/ Pure Snow	*Less Contaminated Snow/Snow-ice mixed debris*	*Debris*	*Non-Snow area/Soil/ Vegetation*	*Unclassified*
Lower Himalaya	24-Dec-2008	0	86.14	0	11.11	2.75
	11-Mar-2009	0	85.97	0	13.94	0.09
Middle Himalaya	13-Dec-2004	0	54.00	0	42.96	3.04
	23-Nov-2005	0	47.27	0	48.66	4.07
Upper Himalaya	03-May-2011	9.17	44.23	24.79	21.75	0.06
	04-Dec-2011	48.45	16.35	22.00	13.04	0.16

Table 2 (c): Land covers classification in (% age) with various statistical models

Study Area	*Date/Month/Year*	*Land Cover Classification in % age (with SVM)*			
		No contamination/ Pure Snow	*Less Contaminated Snow/Snow-ice mixed debris*	*Debris*	*Non-Snow area/Soil/ Vegetation*
Lower Himalaya	24-Dec-2008	0	78.28	0	21.72
	11-Mar-2009	0	80.97	0	19.03
Middle Himalaya	13-Dec-2004	0	68.82	0	31.18
	23-Nov-2005	0	45.24	0	54.76
Upper Himalaya	03-May-2011	23.16	27.94	34.25	14.65
	04-Dec-2011	20.53	47.51	22.48	9.48

Table 2 (d): Land covers classification in (% age) with various statistical models

Study Area	*Date/Month/ Year*	*Land Cover Classification in % age (with MLH)*			
		No contamination/ Pure Snow	*Less Contaminated Snow/Snow-ice mixed debris*	*Debris*	*Non-Snow area/Soil/ Vegetation*
Lower Himalaya	24-Dec-2008	0	72.18	0	27.82
	11-Mar-2009	0	84.84	0	15.16
Middle Himalaya	13-Dec-2004	0	36.78	0	63.22
	23-Nov-2005	0	40.62	0	59.38
Upper Himalaya	03-May-2011	15.19	54.90	23.00	6.91
	04-Dec-2011	16.17	52.12	20.13	11.58

Table 3: Root Mean Square Error (RMSE)

Study area	*Root mean square error (RMSE)*			
	Imagery date	*SAM*	*SVM*	*MLH*
Lower Himalaya	24-Dec-2008	0.10	0.03	0.06
	11-Mar-2009	0.09	0.05	0.06
Middle Himalaya	13-Dec-2004	0.20	0.05	0.08
	23-Nov-2005	0.23	0.04	0.07
Upper Himalaya	03-May-2011	0.09	0.04	0.09
	04-Dec-2011	0.08	0.03	0.10

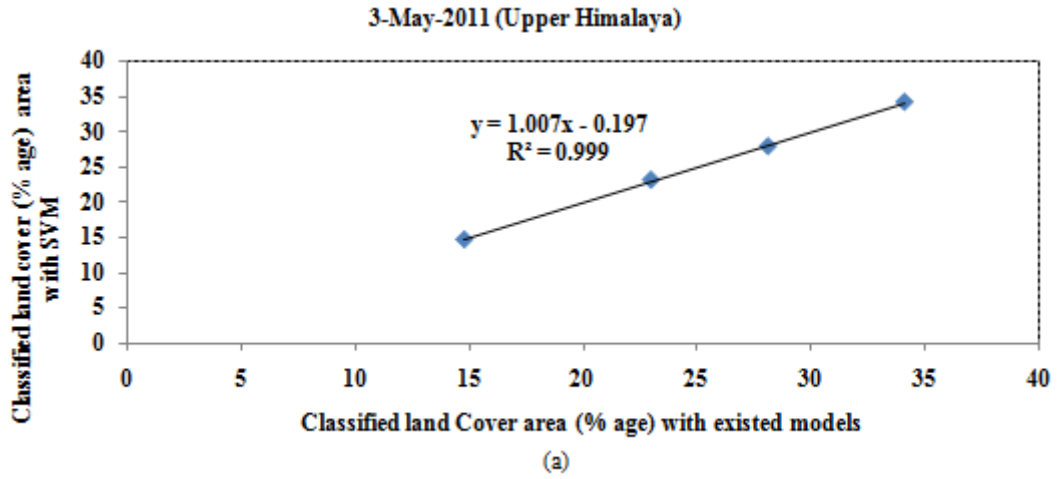

(a)

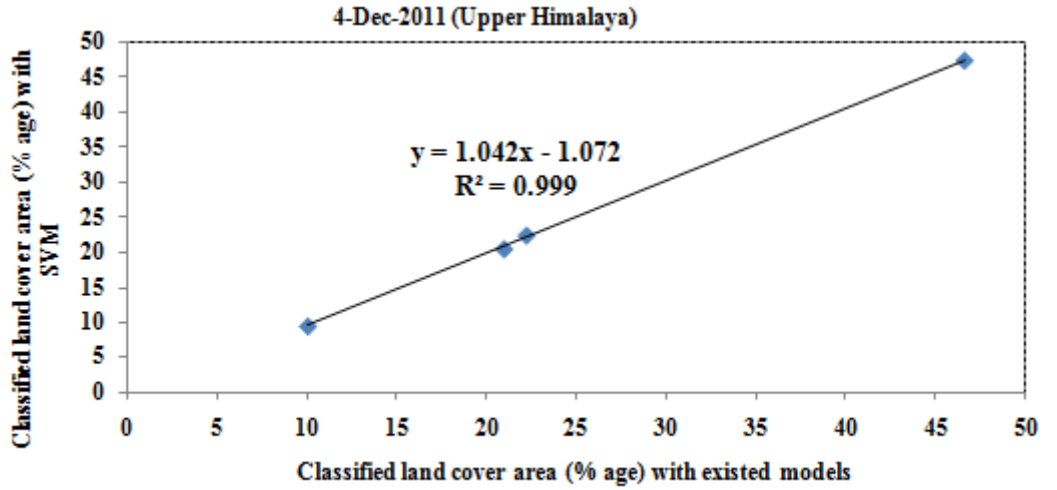

(b)

Figure 6: Comparative and correlation analysis between existed models and SVM with Hyperion data on (a) 3-May 2011 (b) 4-Dec-2011

Acknowledgement

Author's sincere gratitude goes to USGS EROS data center, USA for providing Hyperion images. Thanks are also due to Sh. Aswagausha Ganju Director, Snow & Avalanche Study Establishment (SASE), Defence Research and Development Organization (DRDO), India for providing necessary facilities and for his kind motivation in the field of Geomorphologic research.

References

[1] Assefa M. M., (2004), spatiotemporal dynamics of land surface parameters in the Red River of the North Basin, Physics and Chemistry of the Earth, 29, pp 795–810.

[2] Manjeet Singh., Mishra, V.D., Jyoti Dhar Sharma and Anita Negi., (2012), Estimation of Snow Physical Parameters Using EO-1 Hyperion, IOSR Journal of Applied Physics, 1(6), PP 08-13.

[3] Rogan, J and Chen, D., (2004), Remote Sensing Technology for mapping and monitoring land cover and land-use change, Process in Planning, 61, pp 301-325.

[4] Liang, S., (2004), Quantitative remote sensing of land surfaces. Wiley series in remote sensing, Wiley-Interscience, Hoboken, NJ, XXVI, pp 534.

[5] Metsamaki, S., Vepsalainen, J., Pullinainen, J. and Sucksdorff, Y., (2002), Improved linear interpolation method for the estimation of snow covered area from optical data, Remote Sensing of Environment, 82, pp. 64 – 78.

[6] Haertel, V. F., and Shimabukuro, Y.E., (2005), Spectral linear mixing model in Low spatial resolution image data. IEEE Transactions on Geoscience and Remote Sensing, 43(11), pp 2555 – 2562.

[7] Mishra, V.D., Sharma, J.K., Khanna, R.,(2010), Review of topographic analysis methods for the western Himalaya using AWiFS and MODIS satellite imagery, Annals of Glaciology, 51(54), pp 153-159.

[8] Sharma, S. S., and Ganju, A., (2000), Complexities of avalanche forecasting in Western Himalaya – An overview, Cold Regions Science and Technology,31, pp 95–102.

[9] Manjeet Singh., Mishra, V.D., Thakur, N.K., Kulkarni, A.V., and Mahavir Singh., (2009), Impact of Climatic Parameters on Statistical Stream Flow Sensitivity Analysis for Hydro Power, Journal of Indian Society of Remote Sensing, 37, pp 601–614.

[10] USGS (2003) EO-1 userGuideversion2.3,downloaded2December2012,from ,eo1.usgs.gov/documents/EO1 userguidev2pt320030715UC.pdf.

[11] Pearlman, J.S., Barry, P.S., Segal, C.C., Shepanski, J., Beiso, D., and Carman, S.L., (2003), Hyperion, a Space-Based Imaging Spectrometer, IEEE Transactions on Geoscience and Remote Sensing, 41(6), pp 1160-1173.
[12] Bindschadler, R., and Choi, H., (2003), Characterizing and Correcting Hyperion Detectors Using Ice-Sheet Images, IEEE Transactions on Geoscience and Remote Sensing, 41(6) pp 1189-1193.
[13] ENVI User's Guide (2009) Version 4.7, Research Systems Inc., accessed on 15 July 2012.
[14] Andya, M.R., Singh, R.P., Murali, K.R., Babu, P.N., Kirankumar A.S., and Dadhwal. V.K., (2002), Band pass solar exoatmospheric irradiance and Rayleigh optical thickness of sensors on board Indian remote sensing satellites-1B,1C,1D and P4, IEEE Transactions on Geoscience and Remote Sensing, 40(3), pp 714–718.
[15] Shepherd, J.D., and Dymond, J.R., (2003), Correcting satellite imagery for the variance of reflectance and illumination with topography. International Journal of Remote Sensing, 24(17) pp 3503–3514.
[16] Moran, M.S., Jackson, R.D., Slater P.N., and Teillet. P.M.,(1992), Evaluation of simplified procedures for retrieval of land surface reflectance factors from satellite sensor output. Remote Sensing Environment, 41(2–3), 169–184.
[17] Van der Meer, F., (1996), Spectral mixture modeling and spectral stratigraphy in carbonate lithofacies mapping, ISPRS Journal of Photogrammetric and Remote, 51(3), pp 150–162.
[18] Chavez, P.S.J., (1989), radiometric calibration of Landsat thematic mapper multispectral images, Photogrammetric Engineering and Remote Sensing 55(9), pp 1285–1294.
[19] Kasten, F., (1962), Table of solar altitudes for geographical effect on spectral response from nadir pointing sources. CRREL Spece. Report, pp 57.
[20] Liu, Y., Noumi, Y., and Yamaguchi, Y., (2009), Discrepancy between ASTER- and MODIS-derived land surface temperatures: terrain effects, Sensors, 9(2), pp 1054–1066.
[21] Nichol, J., Hang, L.K., and Sing, W.M., (2006), Empirical correction of low Sun angle images in steeply sloping terrain: a slope-matching technique, International Journal of Remote Sensing, 27(3), pp 629–635.
[22] Anderson, G. P., Pukall, B., Allred, C. L., Jeong, L. S., Hoke, M., Chetwynd, J. H., Adler-golden, S. M., Berk, A., Bernstein, L. S., Richtsmeier, S. C., Acharya, P. K., and Matthew, M. W., (1999), FLAASH and MODTRAN4: state-of-the-art atmospheric correction for hyper spectral data,IEEE Aerospace. Conference. Proceeding, 4, pp 177-181.
[23] Cooley, T., Anderson, G.P., Felde, G.W., Hoke, M.L., Ratkowski, A.J., C hetwynd, J. H., Gardner, J. A., Adler-golden, S. M., Matthew, M. W., Berk, A. ,Bernstein, L. S., Acharya, P. K., Miller, D., and LEWIS, P., (2002), FLAASH a MODTRAN4-based atmospheric correction algorithm, its application and validation, IGARSS,3, pp 1414-1418.
[24] Matthew, M. W., Adler-Golden, S. M., Berk, A., Richtsmeier, S. C., Levine, R. Y., Bernstein, L. S., Acharya, P. K., Anderson, G. P., Felde, G. W., Hoke, M. P., Ratkowski, A., Burke, H.H., Kaiser, R. D., Miller, D. P.,(2000), Status of Atmospheric Correction Using a MODTRAN4-based Algorithm. SPIE Proceedings, Algorithms for Multispectral, Hyper spectral and ultra spectral Imagery, 6, pp 199-207.
[25] Kaufman, Y. J., Wald, A. E., Remer, L. A., Gao, B.C., Li, R.R., and Flynn, L., (1997), The MODIS 2.1-µm Channel-Correlation with Visible Reflectance for Use in Remote Sensing of Aerosol, IEEE Transactions on Geosciences and Remote Sensing, 35, pp 1286-1298.
[26] Justice, C.O., Townshend, J.R.G., Holben, B.N., Tucker, C.J.,(1985), Analysis of the phenology of global vegetation using meteorological satellite data. International Journal of Remote Sensing, 6,pp 1271–1318.
[27] Hall, DK., Riggs, G.A., and Salomonson, V.V., (1995), Development of methods for mapping global snow cover using moderate resolution imaging spectro-radiometer data. Remote Sensing Environtment, 54, pp 127–140.
[28] Kulkarni, A, V., Singh, S.K., Mathur, P., and Mishra, V.D., (2006), Algorithm to monitor snow cover AWiFS data of RESOURCESAT-1 for the Himalayan region. International Journal of Remote Sensing, 27(12), pp, 2449–2457.
[29] Keshri, A.K., Shukla, A., and Gupta, R.P., (2009), ASTER ratio indices for supraglacial terrain mapping International journal of Remote Sensing,30 (2), pp 519-524.
[30] Kruse, F.A. Boardman, J.W., and Huntington, J.F., (2003), Comparison of Airborne Hyper spectral Data and EO-1 Hyperion for Mineral Mapping, IEEE Transactions on Geoscience and Remote Sensing, 41(6), pp 1388-1400.
[31] Richards, J.A., (1999), Remote Sensing Digital Image Analysis, Springer-Verlag, Berlin, pp 240.
[32] Hsu, C.-W., Chang, C.-C., and Lin, C.J., (2007), a practical guide to support vector classification. National Taiwan University.URL http://ntu.csie.org/~cjlin/papers/guide/guide.pdf.
[33] Green, A.A., Berman, M., Switzer, P., and Craig, M.D., (1988), A Transformation for Ordering Multispectral Data in Terms of Image Quality with Implications for Noise Removal. IEEE Transactions on Geoscience and Remote Sensing, 26(1), pp 65-74
[34] Salomonson, V.V., Appel, I., (2004), estimating fractional snow-cover from MODIS using the normalized difference snow index, Remote Sensing of the Environment, 89, pp 351-360.

Author Profile

Manjeet Singh received M. Sc (Physics) degree in 2006 from Gurukul Kangri Vishwavidalaya (Uttrakhand) and pursuing PhD (Physics) from Shoolini University (HP), India and the place of his research work is at Snow & Avalanche Study Establishment (SASE) Chandigarh. During 2006 - 2009, he worked as Junior Research Fellow in SASE a part of Defense Research and Development organization (DRDO) under a collaborative project with Indian Space Research Organization (ISRO), Space Application Centre. His present research interest is geo-spatial modeling of snow physical properties and Himalayan land cover mapping using Remote Sensing and GIS.

Varunendra Dutta Mishra received M. Sc and PhD in condensed matter physics from Indian Institute of Technology, Delhi, India in 1989 and 1996 respectively. He was appointed as a scientist in April 1996 in Snow & Avalanche Study Establishment (SASE) and continuing till now in Chandigarh, India. He has worked in various projects on remote sensing sanctioned by Government of India. . He received various awards like Technology Group Award, Science Day Award, and Best scientific paper award by SASE and Indian Society of Remote Sensing, India. He has published 26 papers in refereed National, International journal and contributed 18 in National and International conferences. His primary research interest is topography and modeling snow physical parameters using optical and passive microwave remote sensing in North West Himalaya.

Narinder Kumar Thakur is currently a Technical Officer 'D' in Snow and Avalanche Study Establishment-Research & Development Centre (SASE-RDC) under Ministry of Defense, Defense Research and Development Organization (DRDO), Chandigarh, India. He has sound knowledge of terrain and snow of North-West Himalayas and he has been associated with the field of remote sensing ever since its inception in SASE. He has immensely contributed in developing a methodology, for identification and mapping of avalanche hazard areas and preparation of Avalanche Hazard Data Cards and Digital Avalanche Atlases for North-West Himalayas, using Remote Sensing and GIS techniques. In recognition of the outstanding contribution and commendable contribution in above, he has been awarded, "Siachen Medal-1991" for serving in highest battle field, DRDO "Best Performance Award - 2001" and "Laboratory Award for DRTC - 2010".

Jyoti Dhar Sharma received the M.Phil degree in Solid State Physics from University of Edinburgh, Scotland (UK) and received PhD (Physics) from HP University, Shimla, India. He has 35 years of teaching experience as a lecture and professor in Department of education, Government of Himachal Pradesh-India. Presently he is working as Professor in Department of Physics, Shoolini University (HP). He supervised M. Phil and PhD scholars. He has published 54 papers in refereed National, International journal and contributed 11 in National and International conferences.